

**Atomic arrangements of quasicrystal bilayer graphene: Interlayer distance expansion**Yuki Fukaya<sup>1,\*</sup>, Yuhao Zhao,<sup>2</sup> Hyun-Woo Kim<sup>3</sup>, Joung Real Ahn,<sup>3</sup> Hirokazu Fukidome,<sup>4</sup> and Iwao Matsuda<sup>2,5</sup><sup>1</sup>*Advanced Science Research Center, Japan Atomic Energy Agency, Tokai, Ibaraki 319-1195, Japan*<sup>2</sup>*Institute for Solid State Physics, The University of Tokyo, Kashiwa, Chiba 277-8581, Japan*<sup>3</sup>*Department of Physics, Sungkyunkwan University, Seobu, Jangan, Suwon, Gyeong Gi-do, Korea*<sup>4</sup>*Research Institute of Electrical Communication, Tohoku University, Sendai, Miyagi 980-8577, Japan*<sup>5</sup>*Trans-scale Quantum Science Institute, The University of Tokyo, Bunkyo-ku, Tokyo 113-0033, Japan*

(Received 30 April 2021; accepted 5 November 2021; published 23 November 2021)

Bilayer graphene exhibits outstanding characteristics that can be modified by adjusting the twist angle between two layers. An exact  $30^\circ$ -twisted bilayer graphene forms a material comprising two-dimensional quasicrystals accompanied by a relativistic Dirac fermion. In this study, the atomic arrangements of quasicrystal bilayer graphene on a SiC(0001) substrate are identified using positron diffraction. The interlayer distance in quasicrystal bilayer graphene is determined to be  $3.46 \text{ \AA}$ , revealing an expansion of  $0.17 \text{ \AA}$  as compared with that of Bernal-stacked bilayer graphene. This result provides important insights for elucidating the origin of the magnitude of coupling between graphene layers.

DOI: [10.1103/PhysRevB.104.L180202](https://doi.org/10.1103/PhysRevB.104.L180202)

Two-dimensional van der Waals (2D-vdW) materials enable the development of versatile structural and electronic properties owing to their stacking degree of freedom. Graphene, a typical example of 2D-vdW material, comprises a honeycomb lattice of  $sp^2$ -hybridized carbon atoms and is renowned for unique characteristics such as massless Dirac electrons [1]. In addition to external factors such as electric fields [2,3] and intercalations [4], the properties of graphene can be significantly modified by the layer number [5], stacking sequence (e.g., AB and AA stacking [6]), and interlayer distance [2].

Recently, the twist angle ( $\theta$ ) between two graphene layers has been identified as an important degree of freedom for controlling the structural and electronic properties of graphene. This finding introduces a research field known as “twistronics” [7]. Typically, graphene layers are stacked onto each other based on  $\theta = 60^\circ$  (AB or Bernal stacking) or  $\theta = 0^\circ$  (AA stacking). When two graphene layers are stacked with twist angles other than  $\theta = 60^\circ$  and  $0^\circ$ , moiré structures with a particular long-range order are formed. At a small twist angle ( $\theta \sim 1.79^\circ$ ), the overlapping of Dirac cones causes van Hove singularities near the Fermi level [8]. In particular, at a certain small twist angle (magic angle), a flat band can be developed at the Fermi level, which forms strongly correlated systems [9]. In practice, a  $1.05^\circ$ -twisted angle results in a superconducting transition at 4 K [10].

It has been suggested that two adjacent honeycomb lattices having an exact  $30^\circ$ -twisted angle form a dodecagonal quasicrystal with 12-fold rotational symmetry (Fig. 1) [11]. The  $30^\circ$ -twisted bilayer graphene provides a class of quasicrystals with a relativistic Dirac fermion. In 2018, exact  $30^\circ$ -twisted bilayer graphene was successfully fabricated over

the entire area of a sample surface, offering a quasicrystal bilayer graphene (QC-BLG) [12]. Promising findings have been reported regarding the peculiar electronic states of Dirac cone replicas in QC-BLG using angle-resolved photoemission spectroscopy (ARPES) [12,13] and tight-binding calculations [14,15], in addition to their dynamics [16]. The origins of these peculiar electronic states have been discussed based on interlayer interactions that have been experimentally argued to be strong coupling [12,13] and decoupling [17,18] regimes. The coupling between layers is the key factor determining the interlayer distance in bilayer graphene [9,15] and remains to be determined. Hence, experimental verification of the interlayer distance enhances the understanding of the unique properties of graphene quasicrystals. In this Letter, we present the unique expansion of the interlayer distance of QC-BLG via total-reflection high-energy positron diffraction (TRHEPD).

Experiments were conducted on an accelerator-based TRHEPD apparatus, which is equipped with reflection high-energy electron diffraction (RHEED) ability at the Slow Positron Facility, KEK (see Ref. [19] for details). The energy of the incident positron beam was set to 10 keV. The diffraction patterns were magnified using a microchannel plate assembly with a phosphor screen and recorded with a charge-coupled-device camera. To measure the rocking curves, the glancing angle of the incident positron beam was varied up to  $6.0^\circ$  in intervals of  $0.1^\circ$  by rotating the sample. All the measurements were performed at room temperature.

Two types of samples were used: QC-BLG and Bernal-stacked bilayer graphene (B-BLG). Both QC-BLG and B-BLG were synthesized on a 4H-SiC(0001) substrate [12,20]. QC-BLG samples were fabricated by replacing single-layer hexagonal boron nitride, which was grown on SiC(0001) substrates with graphene. Sample preparation has been described in detail in other papers [12,21]. The B-BLG samples were

\*fukaya.yuki99@jaea.go.jp

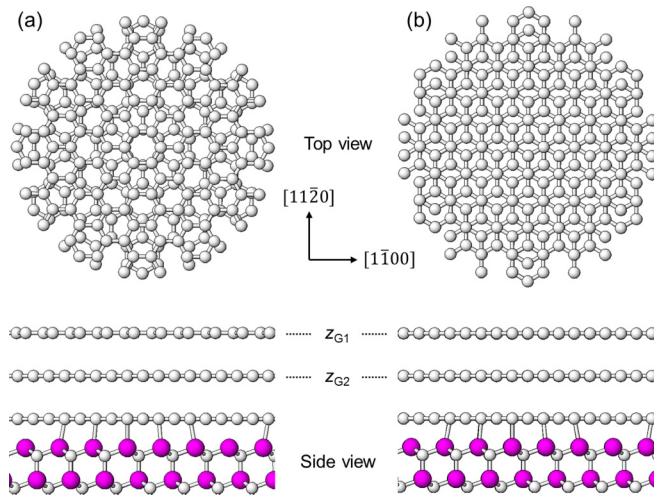


FIG. 1. Structure models of (a) QC-BLG and (b) B-BLG on SiC(0001) substrate. Small gray and large magenta circles denote C and Si atoms, respectively. Only bilayer graphene is depicted in top view.

fabricated using a standard thermal decomposition technique [20]. The formation of bilayer graphene in QC-BLG and B-BLG samples was confirmed directly by cross-sectional transmission electron microscopy [12] and also by observation of Dirac cones in ARPES [12,16].

Figures 2(a) and 2(b) show the RHEED patterns obtained from QC-BLG on the SiC(0001) substrate along the  $[1\bar{1}00]$  and  $[11\bar{2}0]$  directions, respectively. In these patterns, additional diffraction spots and spot intensity changes were observed when compared with the patterns obtained from B-BLG [Figs. 2(c) and 2(d)]. The diffraction spots indexed as  $002\bar{1}$  [Fig. 2(a)] and  $\bar{1}000$  [Fig. 2(b)], defined by four reciprocal lattice vectors for two-dimensional dodecagonal quasicrystal [22], are ascribed to the formation of the upper graphene layer with  $\theta = 0^\circ$ . Hereinafter,  $\theta$  is defined as the

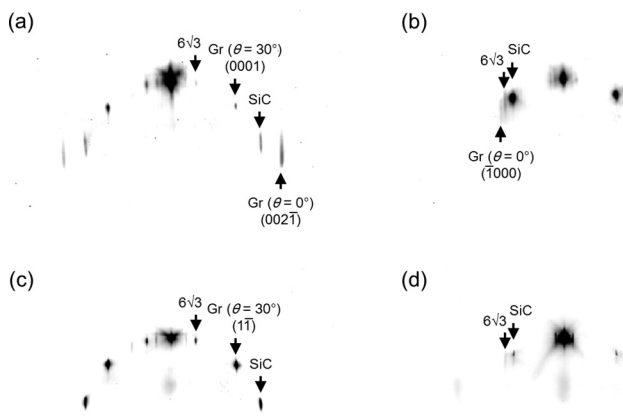


FIG. 2. RHEED patterns obtained from QC-BLG ((a)  $[1\bar{1}00]$  and (b)  $[11\bar{2}0]$ ) and from B-BLG ((c)  $[1\bar{1}00]$  and (d)  $[11\bar{2}0]$ ) on SiC(0001) substrate. Energy and glancing angle of electron beam were 15 keV and  $\sim 4^\circ$ , respectively. In the patterns, “Gr” indicates graphene.

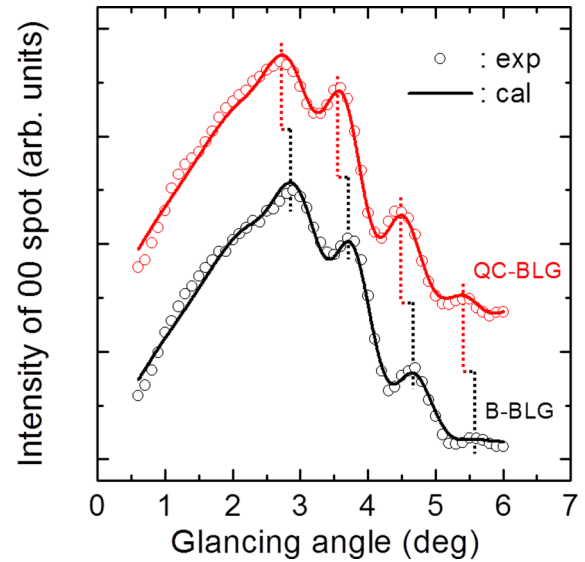


FIG. 3. TRHEPD rocking curves of 00 spot for QC-BLG (red, top) and B-BLG (blue, bottom) on SiC(0001) substrate under one-beam condition. Open circles indicate experimental data. Solid lines denote curves calculated using best-fit parameters. Dotted lines provide visual guide.

twist angle with regard to the unit vectors of SiC(0001). Diffraction spots originating from the SiC(0001), buffer layer ( $6\sqrt{3} \times 6\sqrt{3} - R30^\circ$  superstructure, denoted as  $6\sqrt{3}$ ), and graphene layer with  $\theta = 30^\circ$  were featured in both samples, although the relative intensities varied. It is noteworthy that the 0001 spot for QC-BLG is identical to the  $1\bar{1}$  spots (defined by reciprocal lattice vectors for a general two-dimensional lattice) for B-BLG. Therefore, the observations based on the RHEED patterns correspond significantly to the wide-area formation of QC-BLG on the SiC(0001) substrate.

The rocking curves of 00 (specular) spots for QC-BLG and B-BLG on the SiC(0001) substrates are shown in Fig. 3. The incident beam direction was selected as  $15^\circ$  away from the  $[1\bar{1}00]$  azimuth—this is known as the one-beam condition [23]. Under the one-beam condition, the 00 spot intensity barely depends on the in-plane components of the atomic positions because simultaneous reflections parallel to the surface are suppressed considerably. Hence, the rocking curve contains information regarding the surface-normal atomic positions, i.e., the interlayer distance.

The peak positions and peak magnitudes of QC-BLG and B-BLG differ significantly, although their profiles were similar. Each peak position for QC-BLG shifted toward lower glancing angles compared with those for B-BLG. The kinematical consideration based on the Bragg equation suggests that these shifts were due to the expansion of the interlayer distance in the bilayer graphene for QC-BLG, compared with that for B-BLG.

Figures 4(a) and 4(b) represent the TRHEPD rocking curves from QC-BLG on the SiC(0001) substrate along the  $[1\bar{1}00]$  and  $[11\bar{2}0]$  directions, respectively. The corresponding rocking curves from B-BLG are shown in Figs. 4(c) and 4(d). It is noteworthy that for B-BLG, no reciprocal lattice rods corresponding to  $\bar{1}000$  and  $1000$  for QC-BLG exist

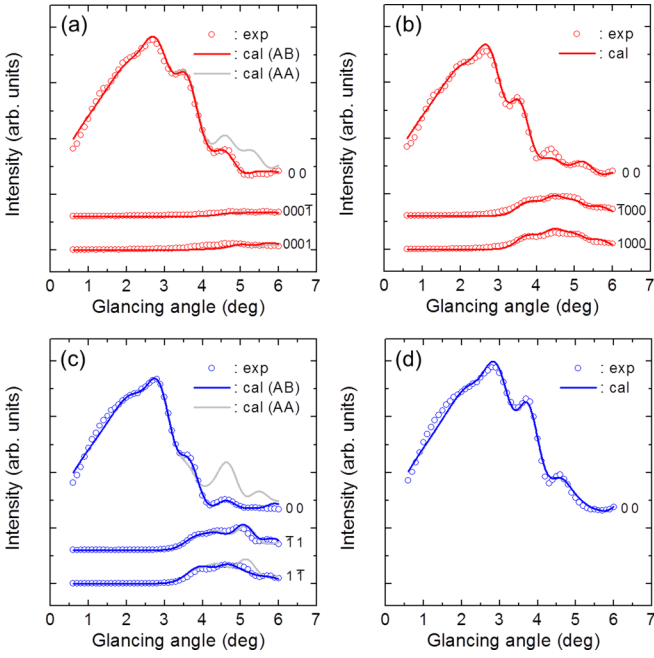


FIG. 4. TRHEPD rocking curves from QC-BLG ((a)  $[1\bar{1}00]$  and (b)  $[11\bar{2}0]$ ) and from B-BLG ((c)  $[1\bar{1}00]$  and (d)  $[11\bar{2}0]$ ) on SiC(0001) substrate. Open circles and solid lines indicate experimental and calculated values, respectively. Thick (red) and thin (gray) lines represent results calculated assuming AB and AA stacking at interface between bottom layer of bilayer graphene and buffer layer of SiC(0001) substrate, respectively.

(see Fig. 2). Except for the peak shifts, the curve shapes for the 00 spots shown in Figs. 4(a) and 4(b) were similar to those shown in Figs. 4(d) and 4(c), respectively. This analogy is associated with the geometrical relationship between the incident beam direction and the crystal orientation of the topmost graphene.

To identify the atomic arrangements of QC-BLG and B-BLG, TRHEPD rocking curve analyses were performed based on dynamical diffraction theory using the multislice method [24]. The heights of the top ( $z_{G1}$ ) and bottom ( $z_{G2}$ ) layers in bilayer graphene from the interfacial Si layer of the SiC(0001) substrate and the corresponding Debye temperatures ( $\Theta_{D1}$  and  $\Theta_{D2}$ ) were regarded as fitting parameters. Notably, because of the limited penetration depth of the positron beam [12,20], the rocking curves were extremely sensitive to the parameters above in the bilayer graphene. For the buffer layer, the heights of C atoms bonded and not bonded to the interfacial Si atoms were fixed at 2.10 and 2.45 Å, respectively [25,26]. The atomic positions and Debye temperature of the 4H-SiC(0001) substrate were fixed based on values in the literature ( $a = 3.073$  Å,  $c = 10.053$  Å,  $\Theta_D = 1300$  K [27]). The absorption potentials of C and Si atoms caused by electronic excitations were set to 0.65 and 0.58 V, respectively [28]. The fitting parameters were optimized to minimize the differences between the experimental and calculated curves. The goodness-of-fit was determined using the reliability factor ( $R$ ) [29].

The solid lines in Fig. 3 represent the TRHEPD rocking curves calculated using the optimum parameters for QC-BLG and B-BLG under the one-beam condition. The calculated curves for both samples coincided with those obtained ex-

TABLE I. Atomic positions and Debye temperatures for QC-BLG and B-BLG on SiC(0001) substrate.

	$z_{G1}$ (Å)	$z_{G2}$ (Å)	$\Theta_{D1}$ (K)	$\Theta_{D2}$ (K)
QC-BLG	$9.26 \pm 0.04$	$5.80 \pm 0.05$	$430 \pm 45$	$637 \pm 196$
B-BLG	$9.07 \pm 0.04$	$5.78 \pm 0.04$	$452 \pm 50$	$420 \pm 101$

perimentally ( $R = 0.64\%$  for QC-BLG and  $R = 0.68\%$  for B-BLG). A summary of the best-fit parameters is presented in Table I. The values of  $z_{G1}$  and  $z_{G2}$  were determined to be  $9.26 \pm 0.04$  Å and  $5.80 \pm 0.05$  Å for QC-BLG, respectively. As for B-BLG,  $z_{G1} = 9.07 \pm 0.04$  Å and  $z_{G2} = 5.78 \pm 0.04$  Å were obtained, which are consistent with those of previous studies within experimental errors [25,26,30,31]. The resultant interlayer distance for QC-BLG and B-BLG were  $3.46 \pm 0.06$  Å and  $3.29 \pm 0.06$  Å, respectively. This yields an expansion of 0.17 Å for the interlayer distance of QC-BLG. However, at the interface, the interlayer distance ( $3.35 \pm 0.05$  Å) between the bottom layer of bilayer graphene ( $z_{G2}$ ) and the buffer layer for QC-BLG was similar to that ( $3.33 \pm 0.04$  Å) of B-BLG, which fits in the interlayer distance of graphite ( $3.35$  Å).

The Debye temperature ( $\Theta_{D1} = 430 \pm 45$  K) of the top layer of QC-BLG is nearly similar to that of B-BLG ( $\Theta_{D1} = 452 \pm 50$  K). The value obtained here matches that of HOPG ( $480 \pm 70$  K) [32], which is also consistent with a previous study [31]. The Debye temperature ( $\Theta_{D2} = 637 \pm 196$  K) of the bottom layer of QC-BLG is higher than that ( $\Theta_{D2} = 420 \pm 101$  K) of B-BLG and is close to that ( $580 \pm 70$  K) reported for graphene/Pt(111) [32]. This suggests the suppression of thermal vibrations, which probably results from the change in the interaction due to the quasicrystallization of bilayer graphene. The Raman spectra demonstrated that the  $ZO'$  mode responsible for layer breathing exhibited a blueshift at a larger twist angle ( $>10^\circ$ ) [33,34]. Thus, in comparison with B-BLG, the large  $\Theta_{D2}$  for QC-BLG is probably important for the blocking of out-of-plane motion due to the twisting of the top graphene layer.

Thus far, there have been no experimental or theoretical reports on the interlayer distance for QC-BLG. However, density-functional theory (DFT) calculations for commensurate phases at around  $\theta = 30^\circ$  showed that the interlayer distance of BLG corresponds to 3.42 Å ( $\theta = 29.4^\circ$  [9]). This value is close to that determined here for the QC-BLG. The slight difference between the values stated in the literature and that obtained here might be the cause for the absence of the SiC substrate in theoretical calculations. The interlayer distance reaches the minimum (3.34 Å) at  $\theta = 60^\circ$  (AB stacking) and maximum (3.61 Å) at  $\theta = 0^\circ$  (AA) [9]. Because the structure of QC-BLG with  $\theta = 30^\circ$  can be termed the intermediate state between AB and AA stacking, the interlayer distance of 3.46 Å obtained for QC-BLG, which is between the minimum and maximum values, is plausible.

To verify the above results, the rocking curves along the  $[1\bar{1}00]$  and  $[11\bar{2}0]$  directions were calculated based on dynamical diffraction theory. For a good approximation, we employed  $91 \times 91$  supercells for QC-BLG and  $13 \times 13$  supercells for B-BLG with respect to the unit cell of graphene.

The stacking sequence of the bottom layer in bilayer graphene and the buffer layer was fixed as the AB-type. For QC-BLG, 45 ( $[1\bar{1}00]$ ) and 35 beams ( $[11\bar{2}0]$ ) lying in the zeroth-order Laue zone were considered in the calculations. For B-BLG, nine beams (both  $[1\bar{1}00]$  and  $[11\bar{2}0]$ ) in the zeroth-order Laue zone were included.

The red and blue solid lines in Fig. 4 outline the rocking curves calculated using the structural and nonstructural parameters determined above for QC-BLG and B-BLG, respectively. The calculations for both samples were for the experiments along the  $[1\bar{1}00]$  ( $R = 0.80\%$  for QC-BLG and  $R = 0.79\%$  for B-BLG) and  $[11\bar{2}0]$  directions ( $R = 0.98\%$  for QC-BLG and  $R = 0.78\%$  for B-BLG). This validates the interlayer distance of QC-BLG determined above and the uniform formation of QC-BLG on the SiC(0001) substrate. When the stacking sequence at the interface was changed from the AB to AA type, the results calculated for both QC-BLG and B-BLG deviated from the experimental profiles, as shown by the gray solid lines in Fig. 4. This verifies that AB stacking was sustained at the interface for QC-BLG. Consequently, owing to quasicrystallization, the interlayer distance in bilayer graphene expanded by  $0.17 \text{ \AA}$  with respect to B-BLG, while the interface structure of the SiC(0001) substrate was maintained.

A unique electronic system of the Dirac cones was identified in QC-BLG, and its origin has been discussed with regard to the interlayer interaction. Various coupling regimes have been reported based on various spectroscopy experiments [12,13,17,18]. In an investigation regarding twisted BLG, the coupling regime was modeled by interactions mediated by moiré (quasi)periodic potentials [35]. Microscopically, the interlayer interaction in the bilayer graphene is controlled by van der Waals forces, whose

treatments remain challenging in first-principles calculations [36]. The precise value of the interlayer distance obtained in the present research facilitates future relevant investigations.

In summary, we determined the atomic arrangements of QC-BLG on the SiC(0001) substrate via TRHEPD rocking curve analysis. We discovered that the interlayer distance of QC-BLG expanded by  $0.17 \text{ \AA}$  compared with that of B-BLG, while the underlying structure remained unchanged. One of the unsolved problems in graphene quasicrystal is the significant difference in Dirac cone replicas between experiment and theory, which considerably hinders the understanding of the peculiar properties of graphene quasicrystal [12]. The interlayer distance expansion of QC-BLG might encourage theoretical scientists to develop relevant models or approaches.

We thank O. Sugino for the insightful discussions and I. Mochizuki and T. Hyodo for their experimental support. Y.F. acknowledges support from JSPS KAKENHI Grants No. JP18H01877 and No. JP19K22134, a research grant from the Murata Science Foundation, and the Toray Science Foundation. J.R.A. was supported by a grant from the National Research Foundation (NRF) of Korea (2021M2E8A1048961). H.F. acknowledges the Strategic Information and Communications R&D Promotion Programme (SCOPE) from the Ministry of Internal Affairs and Communications of Japan, JSPS KAKENHI Grants No. JP19H02590 and No. JP16H06361, and the Murata Science Foundation. I.M. acknowledges JSPS KAKENHI Grants No. JP18H03874 and No. JP19H04398. This study was performed with the approval of the Photon Factory Program Advisory Committee of the Institute of Materials Structure Science (Proposal No. 2017G639).

- 
- [1] K. S. Novoselov, A. K. Geim, S. V. Morozov, D. Jiang, M. I. Katsnelson, I. V. Grigorieva, S. V. Dubonos, and A. A. Firsov, *Nature (London)* **438**, 197 (2005).
- [2] Y. Guo, W. Guo, and C. Chen, *Appl. Phys. Lett.* **92**, 243101 (2008).
- [3] E. V. Castro, K. S. Novoselov, S. V. Morozov, N. M. R. Peres, J. M. B. Lopes dos Santos, J. Nilsson, F. Guinea, A. K. Geim, and A. H. Castro Neto, *Phys. Rev. Lett.* **99**, 216802 (2007).
- [4] S. Ichinokura, K. Sugawara, A. Takayama, T. Takahashi, and S. Hasegawa, *ACS Nano* **10**, 2761 (2016).
- [5] T. Ohta, A. Bostwick, J. L. McChesney, T. Seyller, K. Horn, and E. Rotenberg, *Phys. Rev. Lett.* **98**, 206802 (2007).
- [6] M. Aoki and H. Amawashi, *Solid State Commun.* **142**, 123 (2007).
- [7] S. Carr, D. Massatt, S. Fang, P. Cazeaux, M. Luskin, and E. Kaxiras, *Phys. Rev. B* **95**, 075420 (2017).
- [8] G. Li, A. Luican, J. M. B. L. dos Santos, A. H. C. Neto, A. Reina, J. Kong, and E. Y. Andrei, *Nat. Phys.* **6**, 109 (2010).
- [9] K. Uchida, S. Furuya, J.-I. Iwata, and A. Oshiyama, *Phys. Rev. B* **90**, 155451 (2014).
- [10] Y. Cao, V. Fatemi, S. Fang, K. Watanabe, T. Taniguchi, E. Kaxiras, and P. Jarillo-Herrero, *Nature (London)* **556**, 43 (2018).
- [11] P. Stampfli, *Helv. Phys. Acta* **59**, 1260 (1986).
- [12] S. J. Ahn, P. Moon, T.-H. Kim, H.-W. Kim, H.-C. Shin, E. H. Kim, H. W. Cha, S.-J. Kahng, P. Kim, M. Koshino, Y.-W. Son, C.-W. Yang, and J. R. Ahn, *Science* **361**, 782 (2018).
- [13] W. Yao, E. Wang, C. Bao, Y. Zhang, K. Zhang, K. Bao, C. K. Chan, C. Chen, J. Avila, M. C. Asensio, J. Zhu, and S. Zhou, *Proc. Natl. Acad. Sci. USA* **115**, 6928 (2018).
- [14] G. Yu, Z. Wu, Z. Zhan, M. I. Katsnelson, and S. Yuan, *npj Comput. Mater.* **5**, 122 (2019).
- [15] P. Moon, M. Koshino, and Y.-W. Son, *Phys. Rev. B* **99**, 165430 (2019).
- [16] T. Suzuki, T. Iimori, S. J. Ahn, Y. Zhao, M. Watanabe, J. Xu, M. Fujisawa, T. Kanai, N. Ishii, J. Itatani, K. Suwa, H. Fukidome, S. Tanaka, J. R. Ahn, K. Okazaki, S. Shin, F. Komori, and I. Matsuda, *ACS Nano* **13**, 11981 (2019).
- [17] B. Deng, B. Wang, N. Li, R. Li, Y. Wang, J. Tang, Q. Fu, Z. Tian, P. Gao, J. Xue, and H. Peng, *ACS Nano* **14**, 1656 (2020).
- [18] S. Pezzini, V. Mišeišis, G. Piccinini, S. Forti, S. Pace, R. Engelke, F. Rossella, K. Watanabe, T. Taniguchi, P. Kim, and C. Coletti, *Nano Lett.* **20**, 3313 (2020).
- [19] Y. Fukaya, A. Kawasuso, A. Ichimiya, and T. Hyodo, *J. Phys. D: Appl. Phys.* **52**, 013002 (2019).

- [20] H. Fukidome, Y. Kawai, F. Fromm, M. Kotsugi, H. Handa, T. Ide, T. Ohkouchi, H. Miyashita, Y. Enta, T. Kinoshita, Th. Seyller, and M. Suemitsu, *Appl. Phys. Lett.* **101**, 041605 (2012).
- [21] H.-C. Shin, Y. Jang, T.-H. Kim, J.-H. Lee, D.-H. Oh, S. J. Ahn, J. H. Lee, Y. Moon, J.-H. Park, S. J. Yoo, C.-Y. Park, D. Whang, C.-W. Yang, and J. R. Ahn, *J. Am. Chem. Soc.* **137**, 6897 (2015).
- [22] A. Yamamoto, *Acta Cryst. A* **52**, 509 (1996).
- [23] A. Ichimiya, *Surf. Sci.* **192**, L893 (1987).
- [24] A. Ichimiya, *Jpn. J. Appl. Phys.* **22**, 176 (1983).
- [25] J. D. Emery, B. Detlefs, H. J. Karmel, L. O. Nyakiti, D. K. Gaskill, M. C. Hersam, J. Zegenhagen, and M. J. Bedzyk, *Phys. Rev. Lett.* **111**, 215501 (2013).
- [26] J. D. Emery, V. D. Wheeler, J. E. Johns, M. E. McBriarty, B. Detlefs, M. C. Hersam, D. K. Gaskill, and M. J. Bedzyk, *Appl. Phys. Lett.* **105**, 161602 (2014).
- [27] M. E. Levinshtein, S. L. Rumyantsev, and M. S. Shur, *Properties of Advanced Semiconductor Materials: GaN, AlN, InN, BN, SiC, SiGe* (Wiley, New York, 2001).
- [28] G. Radi, *Acta Cryst. A* **26**, 41 (1970).
- [29] Y. Fukaya, A. Kawasuso, K. Hayashi, and A. Ichimiya, *Phys. Rev. B* **70**, 245422 (2004).
- [30] I. Rizado-Colambo, J. Avila, D. Vignaud, S. Godey, X. Wallart, D. P. Woodruff, and M. C. Asensio, *Sci. Rep.* **8**, 10190 (2018).
- [31] Y. Endo, Y. Fukaya, I. Mochizuki, A. Takayama, T. Hyodo, and S. Hasegawa, *Carbon* **157**, 857 (2020).
- [32] H. Shichibe, Y. Satake, K. Watanabe, A. Kinjyo, A. Kuniyama, Y. Yamada, M. Sasaki, W. W. Hayes, and J. R. Manson, *Phys. Rev. B* **91**, 155403 (2015).
- [33] J. Campos-Delgado, L. G. Cancado, C. A. Achete, A. Jorio, and J.-P. Raskin, *Nano Res.* **6**, 269 (2013).
- [34] R. He, T.-F. Chung, C. Delaney, C. Keiser, L. A. Jauregui, P. M. Shand, C. C. Chancey, Y. Wang, J. Bao, and Y. P. Chen, *Nano Lett.* **13**, 3594 (2013).
- [35] M. Koshino and P. Moon, *J. Phys. Soc. Jpn.* **84**, 121001 (2015).
- [36] F. O. Kannemann and A. D. Becke, *J. Chem. Theory Comput.* **6**, 1081 (2010).